




# Wet-Laid Nonwoven of Activated Carbon Fiber for Gas Adsorption Layer in Face Masks

Yoonjin Kim<sup>1</sup> · Gyu Dong Lee<sup>1</sup> · Song Jun Doh<sup>1</sup> · Jung Nam Im<sup>1</sup> 

Received: 29 November 2022 / Revised: 18 April 2023 / Accepted: 30 May 2023 / Published online: 14 July 2023  
© The Author(s), under exclusive licence to the Korean Fiber Society 2023

## Abstract

In this study, activated carbon fiber (ACF) nonwovens were fabricated using a wet-laid nonwoven process to produce the gas removal layer for a face mask. Two types of polyethylene terephthalate fibers were used as binding fibers. The ammonia gas removal efficiency, mechanical properties, and particulate filtration performances of the fabricated ACF nonwovens were evaluated. The binders did not inhibit the ammonia gas removal efficiency of the ACF. The mechanical properties of the ACF nonwoven fabric could be adjusted based on the amount and composition of the binders. The composite nonwoven, including the ACF nonwoven layer, showed gas adsorption and excellent particulate filtration performances even after exposure to a moist environment. The composite nonwovens seemed to have the potential for a face mask with gas removal characteristics and excellent filtration performances.

**Keywords** Activated carbon fiber · Binder fiber · Wet-laid nonwoven · Gas adsorption · Face mask

## 1 Introduction

Personal protective equipment (PPE) is often used to protect people from infection or injury. PPE may include various items such as gloves, safety shoes or glasses, respirators, body suits, etc. Among them, a facial mask is one of the PPEs to prevent the respiratory system from dust and harmful gasses [1, 2]. Facial masks can be classified into N95/N99/N100 or FFP1/FFP2/FFP3 depending on their particle filtration efficiencies (PFE). Although gas removal efficiency may be very important to facial masks as much as PFE, it has not received sufficient attention. Recently, some facial masks that satisfy both PFE and gas adsorption have been developed using activated carbon powder (ACP) [3, 4].

Activated carbon materials have been used as chemical adsorbents owing to very high specific surface areas and high microporous volumes [5]. Activated carbon materials are available in various forms, such as granules, powders, and fibers. Each type has advantages and disadvantages in terms of cost, production, and adsorption properties [6]. In addition to their macroscopic morphology, ACP and

activated carbon fiber (ACF) differ in their adsorption mechanisms because of their different pore structures. In ACP, gas molecules must first pass through the macropores (widths larger than 50 nm) and then through the mesopores (widths between 2 and 50 nm) before reaching the micropores (widths smaller than 2 nm) due to the hierarchical pore structure. In contrast, numerous micropores of ACF are directly exposed to the surface, and gas molecules are adsorbed rapidly. Therefore, ACF has a faster adsorption rate than the granular and powder form [7–9]. ACF also exhibited superior adsorbent performance compared with zeolites and silica gels [10–16].

Gas adsorbent nonwovens were prepared by scattering ACPs to the needle-punched nonwoven [17, 18] or by carbonizing polyacrylonitrile or cellulose nonwoven to obtain ACF nonwoven fabrics [19]. However, these fabrics are inappropriate for a mask layer because they are thick or because ACP may fall out of the nonwovens. Although ACF has several advantages when used as a thin gas adsorption layer for a face mask, it is not easy to obtain the ACF nonwoven by carding and needle-punching processes due to its fragility and short fiber length.

Nonwovens can be fabricated by various processes, such as wet laid, spunbond (SB), air laid, needle punched, spunlace (SL), and melt-blown (MB). Among the fabricating methods of nonwovens, the wet-laid process is a modified

✉ Jung Nam Im  
founder@kitech.re.kr

<sup>1</sup> Advanced Textile R&D Department, Korea Institute of Industrial Technology, Ansan 15588, Republic of Korea

papermaking process and is characterized by obtaining a product with more uniform pore distribution, enhanced strength, and thin structure compared with other nonwovens [20, 21].

In the case of manufacturing a wet-laid nonwoven with ACF, it is important to select an appropriate bonding method because ACF itself does not have the sufficient self-bonding capability. Binders such as latex and adhesive fibers are usually used to impart mechanical strength to wet-laid nonwoven. Hotmelt adhesive fibers can be used for manufacturing an ACF wet-laid nonwoven because they are partially melted by the heating. Examples of hotmelt adhesive fibers include polyolefins, modified polyesters, and copolyamides [22]. Among them, sheath/core bicomponent fibers are popularly used due to the uniform distribution of adhesive, adding integrity by the remained fiber structure, or cost-effective bonding. A representative sheath/core-type bicomponent fibers are the low-melting polyethylene terephthalate fiber (LMF). The LMF is composed of a core component in polyethylene terephthalate (PET) and a sheath component in a copolyester that has a lower melting point than regular PET.

In this study, ACF nonwovens were prepared by a wet-laid process to obtain a face mask with gas removal efficiency as well as PFE equivalent to an N95 mask. The effect of binders on the properties of the ACF nonwoven, including gas removal efficiency, was thoroughly investigated. In addition, the performances as a face mask were evaluated by examining the characteristics of the composite nonwovens with various ACF nonwovens.

## 2 Experimental

### 2.1 Materials

Viscose rayon-based ACF was purchased from Korea Activated Carbon Fiber Ltd. The average fiber length,

specific area, and micropore diameter of ACF were  $2.25 \pm 1.64$  mm,  $1700 \text{ m}^2/\text{g}$ , and  $18.8 \pm 0.11$  Å, respectively. Binding fibers such as LMF short-cut fibers (2 denier, 6 mm) and PET short-cut fibers (0.7 denier, 5 mm) were purchased from Huvis Ltd. PET SL nonwoven (Baiksan Lintex Co., Ltd.,  $45 \text{ g/m}^2$ ), polypropylene MB nonwoven (Sun Jin Industry Co., Ltd.,  $35 \text{ g/m}^2$ ), and PET thermal bonding (TB) nonwoven (Younatech Co., Ltd.,  $18 \text{ g/m}^2$ ) were used to fabricate the composite nonwoven.

### 2.2 Preparation of ACF Nonwoven and Composite Nonwoven

ACF nonwovens were fabricated using a hand-sheet former with ACF, LMF, and PET at various blend ratios. The ACF and binding fibers were weighed and dispersed in water. Nonwovens were formed on the screen mesh through filtration of the dispersed fibers in water.

The dimension of the wet-laid nonwovens was  $20 \text{ cm} \times 20 \text{ cm}$ . The weight of the ACF was fixed at 0.8 g, which is equivalent to  $20 \text{ g/m}^2$ , for each nonwoven. Binding fibers weighing 0.4/0.8/1.2 g were added to ACF to obtain ACF nonwoven of 30/40/50  $\text{g/m}^2$ , which are referred to as B30, B40, and B50, respectively. The blend ratios of LMF/PET as a binding material were 30/70, 50/50, and 70/30 (w/w), which were named L3P7, L5P5, and L7P3, respectively (Table 1).

After the dewatering process, the wet specimens were dried in a convection oven at  $150 \text{ }^\circ\text{C}$  for 60 min and the thermal bonding process was followed. Thermal bonding was performed using a laminating machine (RPS-L 600 K, MEYER GmbH) at  $120 \text{ }^\circ\text{C}$  and  $39 \text{ N/cm}^2$ .

The composite nonwovens having a multi-layered structure for a face mask were fabricated by sequentially stacking SL nonwoven, ACF nonwoven prepared, MB nonwoven, and TB nonwoven (Fig. 1).

**Table 1** Blend ratio and basis weight of ACF nonwoven

Sample	Weight of ACF (g)	Weight of binders (g)		Blend ratio of binders (wt%)		Basis weight ( $\text{g/m}^2$ )
		LMF	PET	LMF	PET	
L3P7B30	0.8	0.12	0.28	30	70	30
L5P5B30	0.8	0.20	0.20	50	50	30
L7P3B30	0.8	0.28	0.12	70	30	30
L3P7B40	0.8	0.24	0.56	30	70	40
L5P5B40	0.8	0.4	0.4	50	50	40
L7P3B40	0.8	0.56	0.24	70	30	40
L3P7B50	0.8	0.36	0.84	30	70	50
L5P5B50	0.8	0.6	0.6	50	50	50
L7P3B50	0.8	0.84	0.36	70	30	50



**Fig. 1** Cross-sectional image of the composite nonwoven

## 2.3 Morphological Characterization

The morphology of the ACF nonwovens was evaluated using field-emission scanning electron microscopy (FE-SEM; Hitachi SU-8010, Hitachi High Technologies Co., Japan). The ACF nonwovens were sputter-coated with gold for 200 s with a current of 15 mA prior to imaging and microstructure analysis.

The pore characteristics were measured using a capillary flow porometer (CFP-1500AEX, Porous Materials Inc.). Pore size analysis was performed according to ASTM F316-01. For the wet samples, we used Galwick™ solution with a surface tension of 15.9 dyne/cm to fill the pores of the nonwovens. The mean and bubble pore sizes of the three samples were determined.

## 2.4 Mechanical Properties

### 2.4.1 Dimensional Stability

The dimensional stability was evaluated by measuring the extent of shrinkage during the drying process. The areas of the ACF nonwoven were measured before and after the drying process. The shrinkage ratio (%) was calculated using Eq. (1).

$$\text{Shrinkage ratio (\%)} = (A_0 - A_h) / A_0 \times 100, \quad (1)$$

where  $A_0$  and  $A_h$  are the areas of the specimen before ( $A_0 = 20 \text{ cm} \times 20 \text{ cm}$ ) and after drying, respectively. Three samples of each ACF nonwoven were used for the dimensional stability tests.

### 2.4.2 Tensile Strength

The tensile strengths were measured using a tensile tester (Instron 3343, Illinois Tool Works Inc., USA). The ACF nonwoven was cut to dimensions of 2 cm (width)  $\times$  10 cm (length). The test was performed with a gauge length of

50 mm and a constant elongation rate of 50 mm/min. Five samples of each nonwoven were used for the tensile strength tests.

### 2.4.3 Stiffness

The stiffness was evaluated using a Gurley stiffness tester based on the Test Method TAPPI T 543 om-11. A sample (2.5 cm  $\times$  2.5 cm) was attached to a clamp such that 6.4 mm of the sample, held in the jaws, overlapped the top of the pendulum pointer. The clamp arm brought the sample into contact with the top of the pendulum, and the bending resistance was measured at the point where the sample cleared the pendulum.

### 2.4.4 Ammonia Gas Removal Efficiency

The ammonia gas removal efficiency was measured based on JIS K 0804:2014 (gas detector tube measurement system) using ACF in a polyethylene teabag [23, 24]. Re-dried ACF (r-ACF) specimens were prepared by drying the wet ACF; ACF was immersed in distilled water for approximately 5 min and the wet ACF was dried in a convection oven at 150 °C for 60 min. For the ACF nonwoven and composite nonwoven fabrics, wet nonwovens were cut into 10 cm  $\times$  10 cm pieces before the drying process. Thermal bonding was carried out before the ammonia gas removal test was performed.

To assess the ammonia gas removal efficiency, specimens were placed into a 2 L test chamber under the following test conditions: temperature of  $23.0 \pm 2.0$  °C and humidity of  $65 \pm 20\%$  RH. To adjust the concentration to 100 ppm, 10  $\mu\text{L}$  of 10 v/v% ammonia solution was injected into the 2 L test chamber. After predetermined periods (30, 60, 90, or 120 min) following the injection of ammonia solution, 50 mL of gas from the 2 L test chamber was drawn into the gas detection tube (GASTEC, 3La) using a gas detection pump (GASTEC, GV-110S). The concentration of ammonia gas was calculated based on the color change of gas detection tube.

A control test was performed without a sample by following the same process as described above. The concentrations of ammonia gas in the 2 L test chambers were measured after 120 min and the removal efficiency of ammonia gas was calculated using Eq. (2).

$$\text{Ammonia gasremoval efficiency (\%)} = (C_o - C_s) / C_o \times 100, \quad (2)$$

where  $C_o$  is the gas concentration in the control chamber after 120 min, and  $C_s$  is the gas concentration in the sample chamber after 120 min. Three samples of each specimen were tested to measure the removal efficiency of the gas.

### 2.4.5 Filtration Performances

The particle filtration efficiency (PFE) and airflow resistance of the ACF nonwovens and composite nonwovens were measured using an automated filter tester (TSI 8130, TSI Inc., USA) based on 42 CFR (Code of Federal Regulations) 84 of the National Institute for Occupational Safety and Health (NIOSH) standard [25]. After fixing the test fixture, the PFE and airflow resistance were measured at an airflow rate of 85 L/min. A neutralized polydisperse solid NaCl aerosol with a mass median diameter of 0.26  $\mu\text{m}$  and count median diameter of 0.075  $\mu\text{m}$  was used as the test aerosol.

### 2.4.6 Humidification

Humidification of the ACF nonwovens and composite nonwovens was performed in a climate chamber (SH-CTH-1200SCR2, Samheung Energy Co., Korea) under the conditions of  $38 \pm 2.5$  °C,  $85 \pm 5\%$  RH, for 24 h.

## 3 Results and Discussion

### 3.1 Effect of ACF Content on Removal Efficiency of Ammonia Gas

ACF nonwovens as a gas removal layer for a face mask were prepared using a wet-laid nonwoven process. The relationship between the amount of ACF and ammonia gas removal efficiency was evaluated to determine the appropriate ACF content in the nonwovens. During the wet-laid nonwoven process, the ACF is dispersed in water and subsequently dried. Therefore, it is necessary to investigate the effect of the wetting procedure on the gas adsorption of ACF.

Figure 2 shows the ammonia gas removal efficiency depending on the amount of ACF in the dry ACF (d-ACF) and r-ACF; the latter denotes a specimen that undergoes the wetting and subsequent drying procedures, thus simulating a wet-laid nonwoven process. As shown in Fig. 2, the ammonia gas removal efficiency increased up to 60 min, and after which equilibrium was reached. The d-ACF sample consistently exhibited a higher value than the r-ACF sample for the same amount of ACF even after reaching equilibrium. Additionally, the ammonia gas removal efficiency also tended to increase as the amount of ACF increased.

Fabrics with more than 70% ammonia removal efficiency are regarded after 120 min as deodorant fabrics [26]. In the case of d-ACF, the removal efficiency was  $\geq 70\%$  when evaluated with a specimen with ACF content of  $\geq 0.06$  g. In contrast, in the case of r-ACF, the removal efficiency was  $\geq 70\%$  when the amount of ACF was  $\geq 0.2$  g. Therefore, it seemed preferable to use 0.2 g of ACF in the case of ACF nonwovens produced by the wet-laid process. This corresponds to

20 g/m<sup>2</sup> based on 100 cm<sup>2</sup> of the nonwoven area used for testing the ammonia gas removal efficiency.

Figure 3 shows the effect of drying time on the ammonia gas removal efficiency of the r-ACF specimens. Wet ACF nonwovens were dried at 150 °C for 10, 30, 60, 120, and 180 min after the wet-laying process (wetting and dewatering) using 0.2 g of dry ACF. The ammonia gas removal efficiency increased until 60 min, after which no further increase was observed with a prolonged drying time.

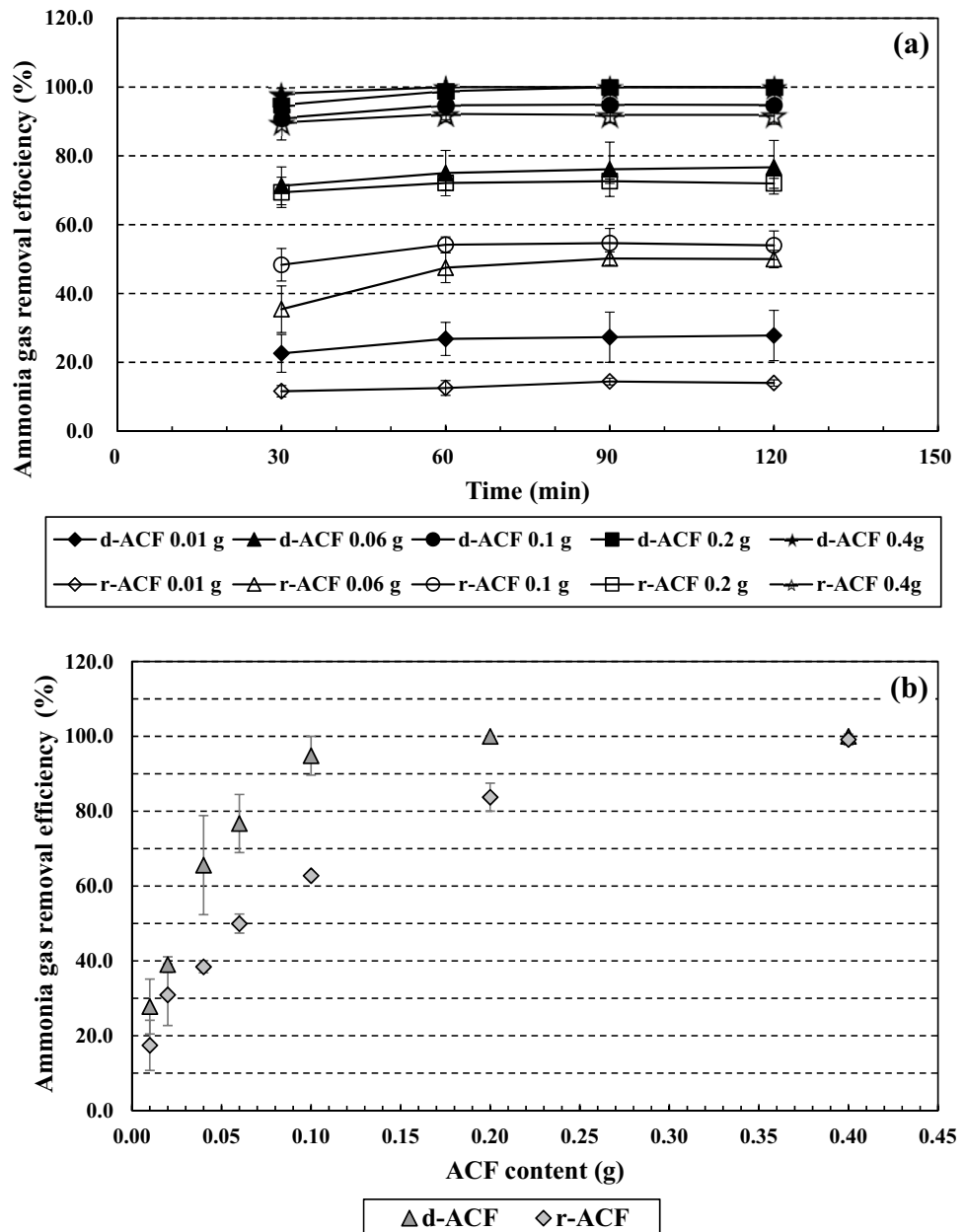
A decrease in the ammonia gas removal efficiency of the r-ACF implies that a change in the micropores occurred during the wetting process, because gas adsorption occurs primarily in the micropores of the ACF. During the 60 min of the drying stage, the evaporation of water from the ACF seemed to increase the ammonia gas removal efficiency. However, despite prolonged drying for 180 min, the ammonia gas removal efficiency did not increase to its original level (d-ACF). It seemed that the moisture in the micropores of ACF inhibited the physical ammonia gas adsorption and also affected the surface chemical characteristics of ACF relating to its affinity to ammonia gas [27–29]. Further studies are needed to clarify this more accurately. Based on the relationship between drying time after the wetting process and gas removal efficiency, the drying conditions for the wet-laid nonwoven process were fixed at 150 °C for 60 min.

### 3.2 Morphologies of ACF Nonwovens

In this study, wet-laid nonwovens composed of ACF, LMF, and PET were prepared. Figure 4 presents the representative surface and cross-sectional SEM images of the ACF nonwoven. The ACF and binder fibers seemed to be dispersed well. In the case of ACF(i), unique wrinkled surface characteristics appeared because a viscose rayon-based ACF was used in this study. PET(ii) and LMF(iii) showed a smooth surface, and intra-fiber bonding, formed by partial melting of LMF (iii) during the drying step, was observed. LMF(iii) fiber used in this study is composed of PET, melting at high temperature of 250 °C, as a core component and copolyester with a broad melting point of approximately 110–170 °C as a sheath component. Therefore, the partial melting could occur at the sheath part of LMF without a remarkable change in the core component during the drying step of 150 °C, which seemed to induce an intra-fiber bonding instead of film formation by complete melting of LMF.

Figure 5 shows the mean pore sizes and bubble point pore sizes of the various ACF nonwovens. Both the mean and bubble point pore sizes tended to decrease with an increase in the basis weight. An increase in the basis weight indicated an increase in the number of fibers per unit area. This increase in the nonwoven density could result in a decrease in the pore size. Additionally, a decrease in pore size was also observed when the proportion of LMF in the binder

**Fig. 2** Ammonia gas removal efficiency according to ACF content: **a** removal efficiency over time, and **b** efficiency after 120 min of adsorption



increased. It seemed to be caused by the partial melting that happened only in the sheath component of LMF, as shown in Fig. 4. It was because the drying and bonding temperatures were much lower than the melting point of the core component of LMF, and were in the middle of a broad melting point of the sheath component of LMF. The partial melting of the LMF flattened it a little, and the melted part seemed to penetrate the space between the fibers of the nonwoven, which resulted in a decrease in the pore size. However, there was no dramatic change in the mean pore size depending on the LMF portion of the binders. It seems to happen because the sheath part of LMF was a small portion of the total ACF nonwoven.

### 3.3 Dimensional Stability of ACF Nonwovens

ACF is short and fragile, which makes it difficult to convert it into a sole component nonwoven fabric. It can be resolved by consolidating nonwoven structures with the use of binding fibers. However, shrinkage can occur owing to heat during the drying or thermal bonding step.

Figure 6 shows that the shrinkage ratio increased proportionately with an increase in the LMF content. As the basis weight increased, the shrinkage ratio tended to increase. It implies that the amount of LMF had a significant effect on the shrinkage of the ACF nonwoven while the PET binder contributed to the dimensional stability of ACF



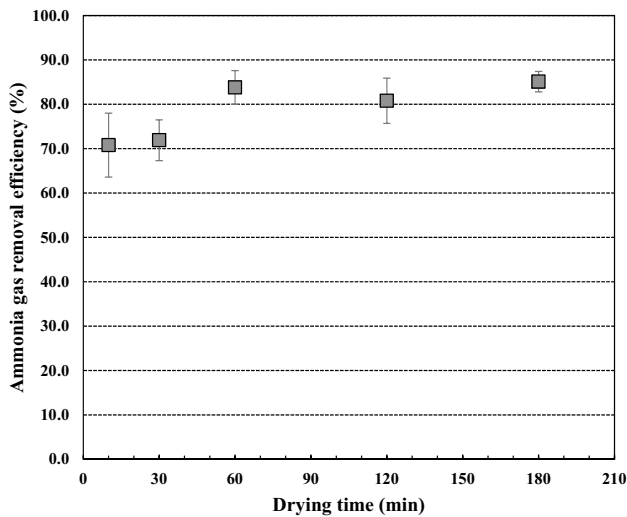


**Fig. 3** Ammonia gas removal efficiency of r-ACF against drying time

nonwoven. In the case of LMF binder, the sheath component is a copolyester with a low melting point of approximately 110–170 °C; it is prone to shrinkage when heated, as the oriented structure turns into a random coil structure. In contrast, PET binder was expected to be affected to a significantly lesser extent by the drying temperature because it

has a much higher melting point than the drying or thermal bonding temperature.

### 3.4 Tensile Strength and Stiffness of ACF Nonwovens

Mechanical properties are one of the criteria in face masks. Tensile strength is important because it could affect the resistance to external stimuli and processability. Stiffness is closely related to the improvement of wearing comfort by securing an internal space of the mask. The effects of the binders on the tensile strength and stiffness of the ACF nonwovens were investigated. Figure 7 shows that the tensile strength and stiffness of the ACF nonwovens increased with increase in the LMF content in the binders or the basis weight. As the LMF content increased, the partial melting of LMF during the heating process seemed to enhance the bonding strength between the fibers.

In general, the weakest layer of a face mask is the filter layer. The tensile strength of the MB nonwoven used for preparing the composite nonwoven in this study was  $6.98 \pm 0.07$  N/20 mm. At 30 g/m<sup>2</sup>, the tensile strength of the ACF nonwoven was lower than that of the MB nonwoven, regardless of the blend ratio of the LMF and PET. In addition, the L3P7B40 nonwoven (40 g/m<sup>2</sup> nonwoven with

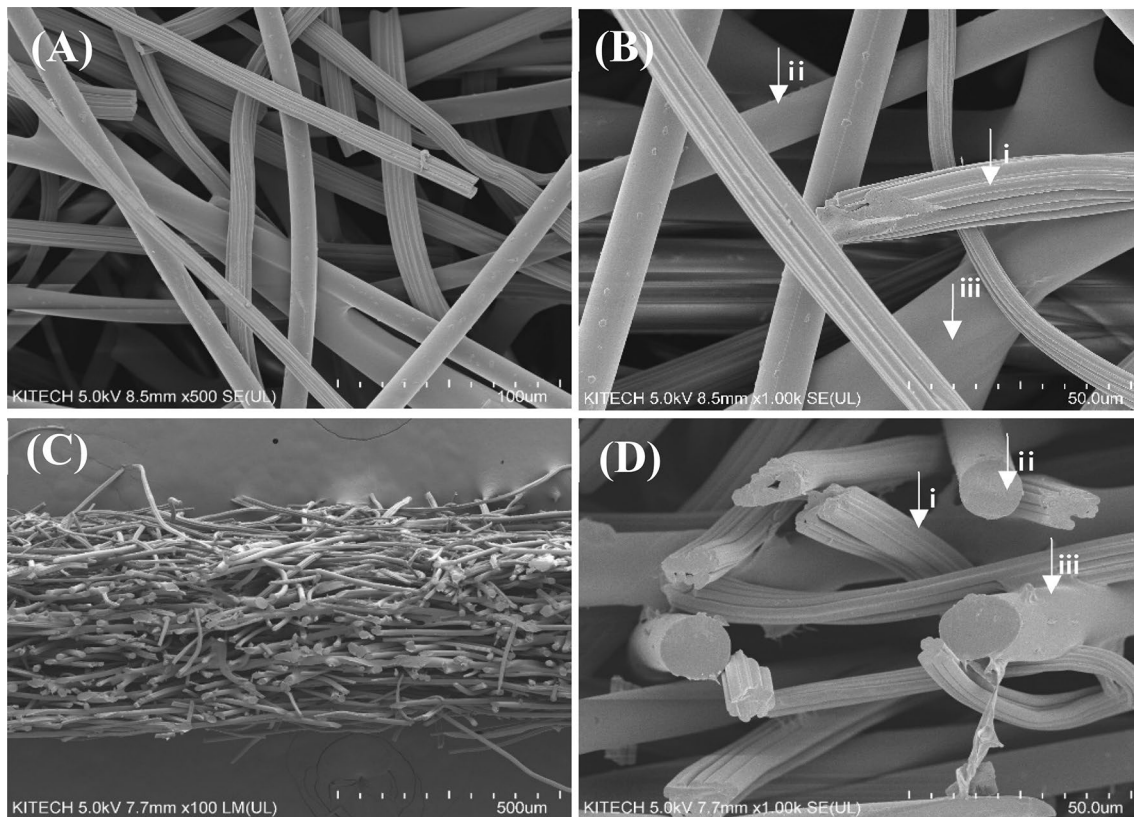


**Fig. 4** Surface (A and B) and cross-sectional (C and D) SEM images of L5P5B40 nonwoven. Arrows indicate (i) ACF (ii) PET (iii) LMF

**Fig. 5** **a** Mean pore and **b** bubble point pore sizes of ACF nonwovens

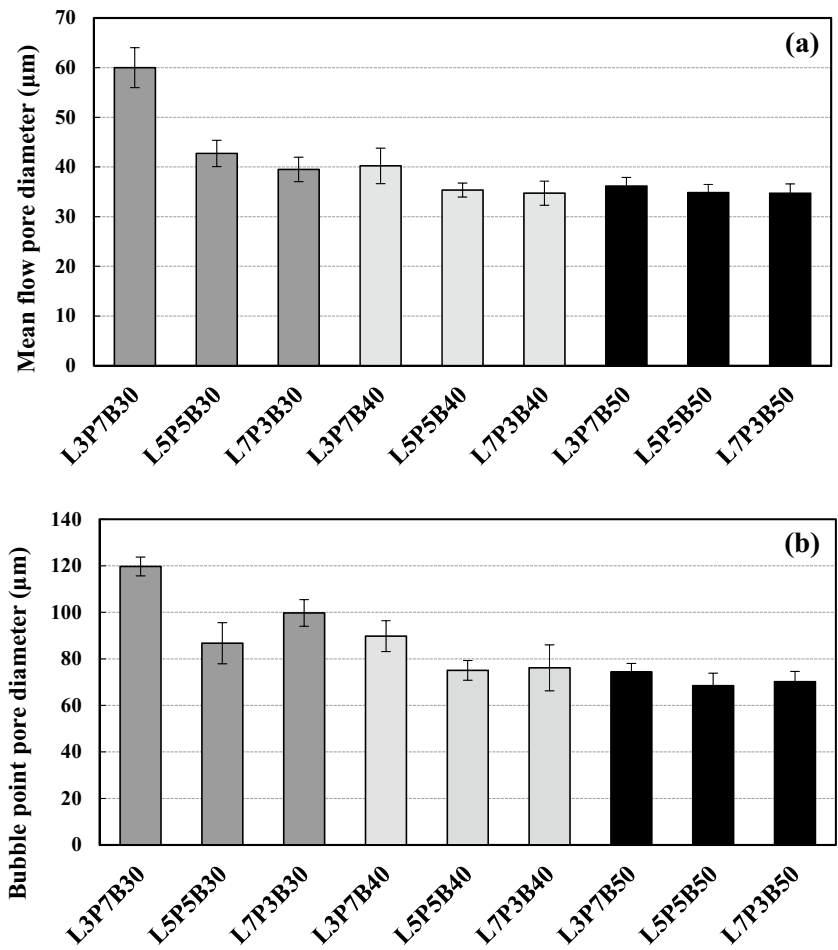
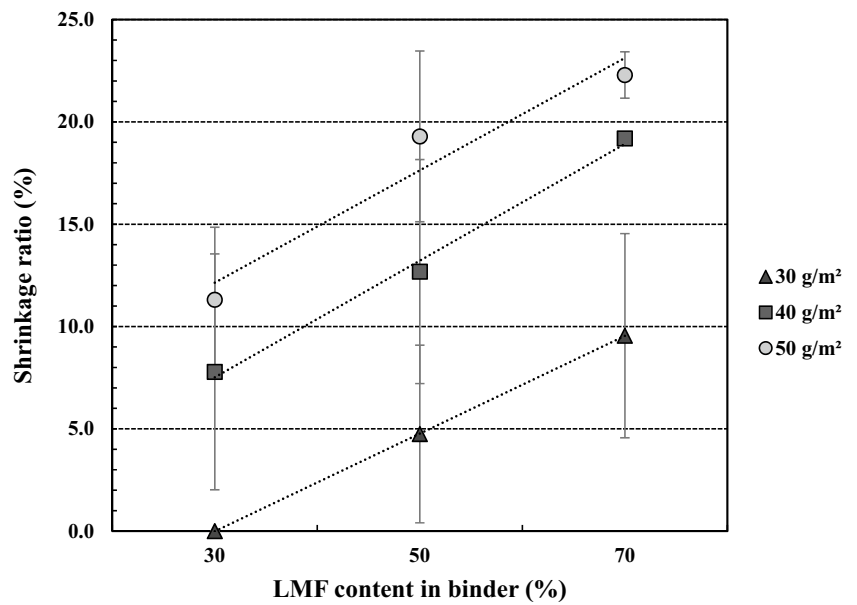


**Fig. 6** Shrinkage ratio of ACF nonwovens according to the fraction of LMF in binder



30% LMF in the binder) also showed lower tensile strength than that of the MB nonwoven. Weaker strength than MB nonwoven may restrict the process applicability. It seemed

that the proportion of LMF, significantly contributing to the bonding strength, in L3P7B40 nonwoven was too low to impart sufficient bonding strength. The ACF nonwoven

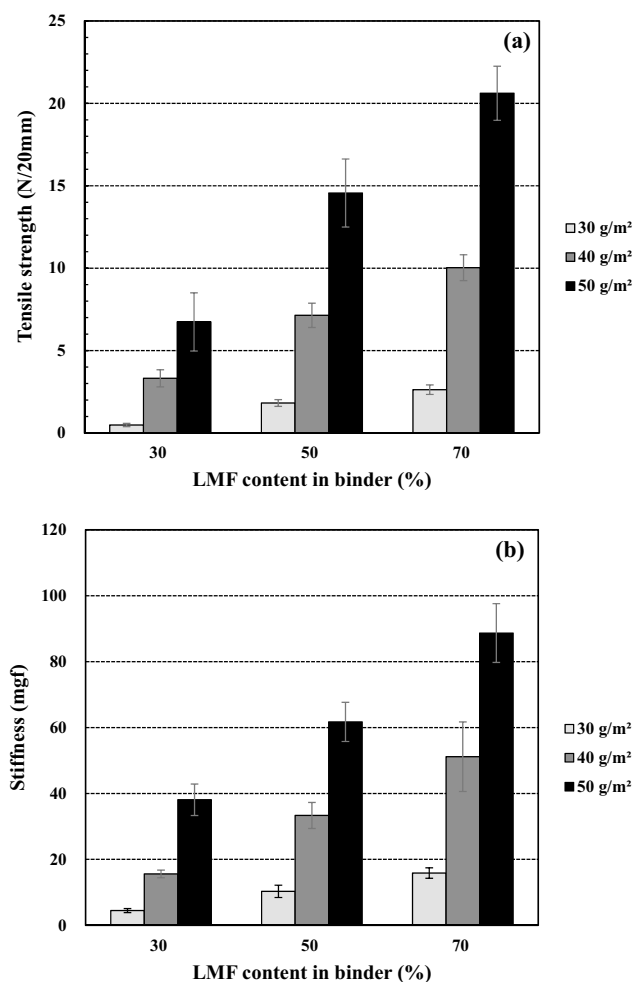


**Fig. 7** Mechanical properties of ACF nonwovens according to LMF content in the binder: **a** tensile strength, **b** stiffness

with more than 50% binder content seemed to be appropriate for air filtration materials from the point of mechanical strength.

The change in stiffness according to the LMF content and basis weight showed a similar trend to that of the tensile strength. With the increase of LMF content or basis weight, the stiffness increased linearly. Intra-fiber bonding by partial melting of LMF seemed to restrict the mobility of fibers, which induced the increase of stiffness. It is advantageous to secure a large area of the mask which is not in contact with the face for better breathability as a duckbill face mask. The outer layer of a face mask, protecting the filter layer, is generally stiffer than the filter layer but the stiffness is not sufficient to secure the shape of a mask. A stiff layer such as high-denier PP spunbond is occasionally adopted to prevent the collapse of the mask shape during breathing. Except for L3P7B30, all the ACF nonwovens showed much higher stiffness than SL ( $7.3 \pm 3.0$  mgf) and TB layer ( $7.4 \pm 4.1$  mgf). The ACF nonwovens having high stiffness

with a high content of LMF are expected to ensure the shape of the face masks remains stable while wearing a face mask.

### 3.5 Ammonia Gas Removal Efficiency of ACF Nonwovens

The binders used in this study do not have gas adsorption capability, and the melting of binders may cause clogging of the micropores of ACF. It may induce a reduction in the ammonia removal efficiency of ACF. To evaluate the effect of the binders on the gas removal efficiency, the amount of ACF was fixed at 0.2 g per 100 cm<sup>2</sup> and the binder content and blend ratio of the binder were selected as variables. As shown in Fig. 8, the ammonia gas removal efficiencies of the ACF nonwovens ranged between 80 and 87%, regardless of the binder content or binder blend ratio, which is similar to the value of the r-ACF 0.2 g specimen. It means that partial melting of LMF did not occur enough to significantly reduce the micropores of ACF to impair the ammonia gas removal efficiency.

While wearing a face mask, the mask is exposed to moisture coming out from a mask wearer. One of the crucial requirements for face masks as PPE is maintaining performance after humidification. For that reason, the effect of moisture on ammonia gas removal was investigated with LMF/PET 5/5 ACF nonwovens after the humidification. The humidification conditions are specified in the test procedure of NIOSH against N95 series filters. As shown in Fig. 9, the ammonia gas removal efficiency of the humidified ACF nonwovens was slightly lower than that of the ACF nonwovens not subjected to humidification. Interestingly, the difference in the ammonia gas removal efficiency before and after humidification tended to decrease as the basis weight increased. It was estimated that as the content of the hydrophobic binders increased, the thickness and hydrophobicity of the nonwoven ACF increased, which made it difficult for moisture to penetrate the nonwoven fabric.

### 3.6 Filtration Performance of ACF Nonwovens

To evaluate the ACF nonwovens as a component of the face mask, the filtration performances of the ACF nonwovens were investigated. As shown in Fig. 10a, the PFE of the ACF nonwovens tended to increase with the increase in the binder content, but the blend ratio of the binders did not have a significant effect on the PFE of the ACF nonwovens.

It is known that aerosol particles are removed from the air stream by fibers through interception, diffusion, inertial impaction, electrostatic deposition, etc. [30]. In the case of filtration mechanism of nonwoven media, the quantity of fibers or the density of the nonwoven in the direction of airflow is likely to affect the PFE. It can be inferred that the number of fibers is affected by the basis weight than



**Fig. 8** Ammonia gas removal efficiency of ACF nonwovens

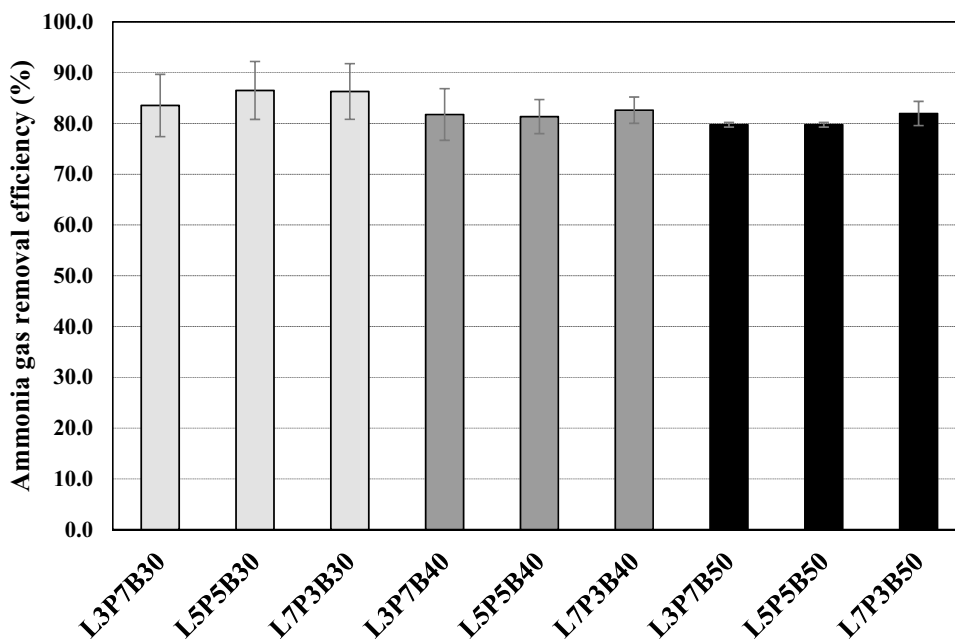
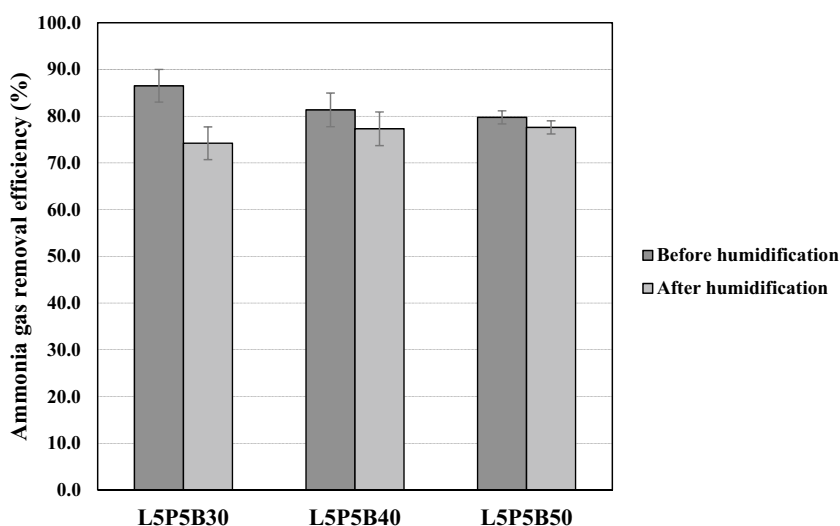


**Fig. 9** Effect of moisture on the ammonia gas removal efficiency of ACF nonwovens



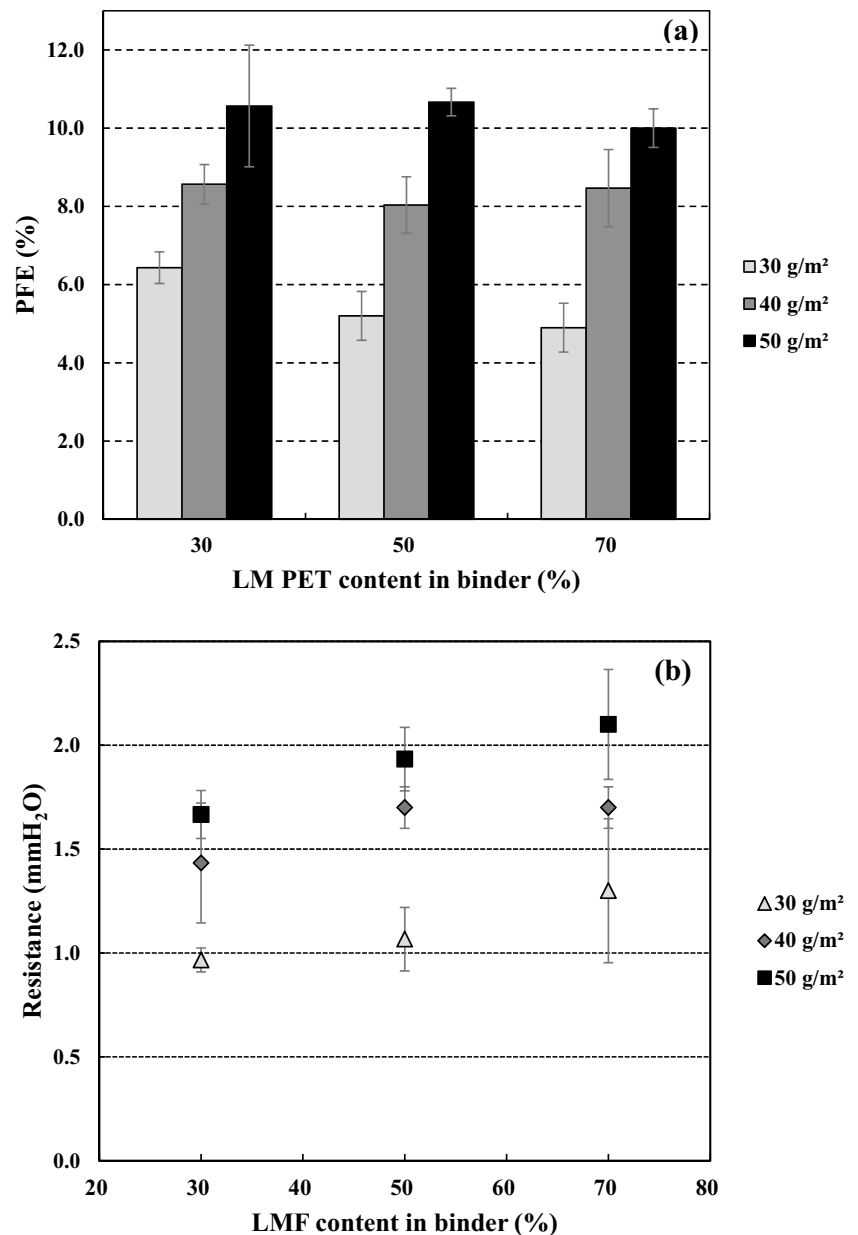
by the LMF content in the binders. Therefore, the increase in the basis weight appeared to increase the number of fibers in the direction of the airflow, which resulted in an increase in the PFE through the interception or impaction mechanism. In contrast, the LMF content in the binder had little effect on the PFE.

The airflow resistance of the ACF nonwovens increased with increase in the basis weight and LMF content in the binders (Fig. 10b). The airflow resistance is also closely related to the mean pore size. As explained in Fig. 5, an increase in the basis weight or the proportion of LMF in the binder resulted in the decrease of mean pore size. It seemed to induce an increase in the airflow resistance.

### 3.7 Filtration Performances and Gas Removal Efficiency of the Composite Nonwovens

In general, N95 masks are composed of an outer layer, a filter layer, and an inner layer. ACF nonwoven showed too low PFE to be used as a filter layer alone. The particulate filtration performances of the composite nonwovens, including the ACF nonwovens, were evaluated. The composite nonwovens were prepared with SL nonwoven as an outer layer, ACF nonwoven as a gas removal layer, MB nonwoven as a filter layer, and TB nonwoven as an inner layer (Fig. 1). Figure 11 showed the filtration performances of composite nonwovens.

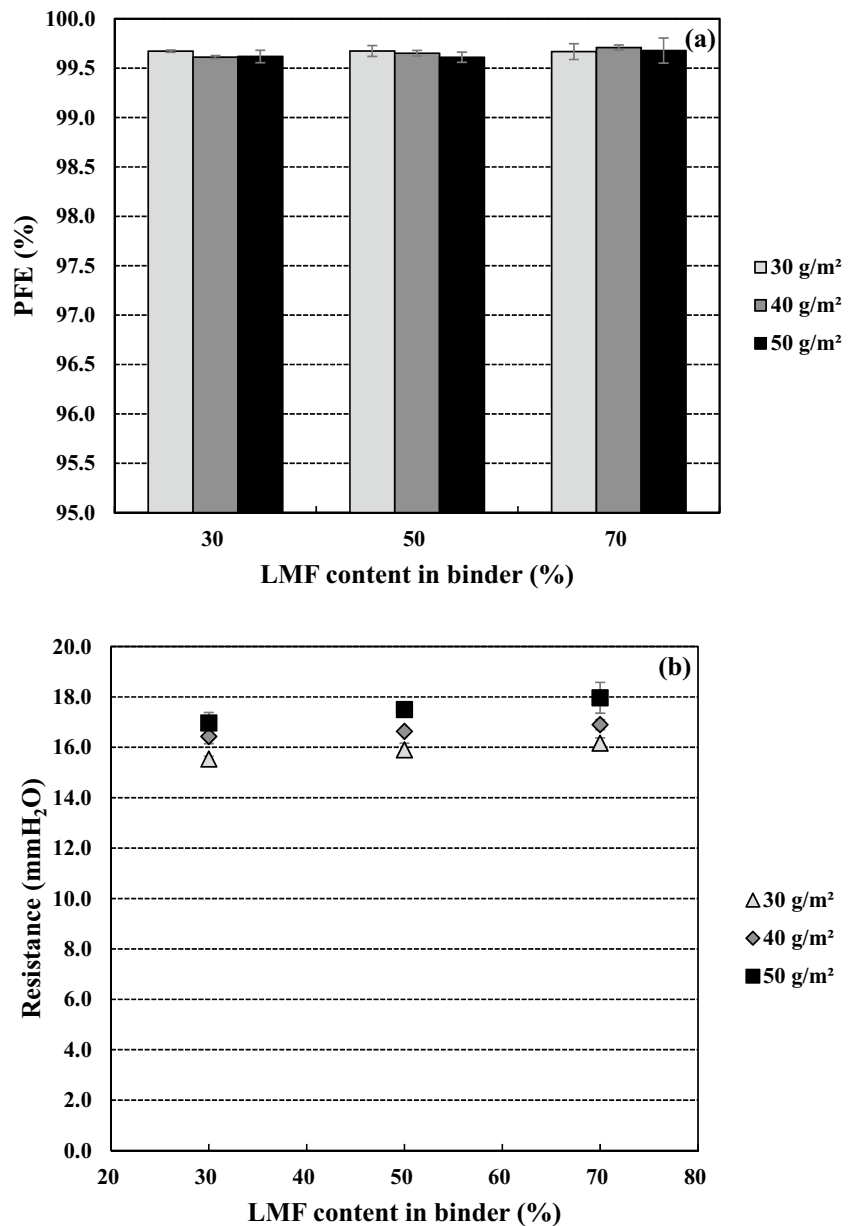
**Fig. 10** **a** PFE and **b** airflow resistance of ACF nonwovens according to LMF content in the binder



The PFE of the composite nonwovens seemed not to be deteriorated by the addition of ACF nonwoven layer because the PFE of MB nonwoven was very high. It means that the addition of ACF nonwoven layer did not affect the filtration capacity of MB nonwoven layer. The airflow resistance of the composite nonwovens tended to increase slightly with the increase in the basis weight and LMF portion in the binders of the ACF nonwoven. The PFE and airflow resistance of the composite nonwovens were  $\geq 99.5\%$  and 14–18 mm H<sub>2</sub>O, respectively. These values were similar to those of composite nonwovens without ACF layers (PFE of 99.7% and airflow resistance of 15.8 mm H<sub>2</sub>O). This indicates that ACF nonwovens do not impair the particulate filtration performance of the materials.

The effect of moisture on the particulate filtration performance of composite nonwovens was also investigated. The composite nonwovens comprising ACF nonwoven with LMF/PET 5/5 binders were exposed to humidification. As shown in Fig. 12, even when the ACF nonwoven layer was added, humidification did not deteriorate the particulate filtration performance. Figure 13 shows the ammonia gas removal efficiency of the composite nonwovens. All the composite nonwovens showed similar ammonia gas removal efficiency to sole ACF nonwovens, as shown at Fig. 9.

**Fig. 11** **a** PFE and **b** airflow resistance of the composite nonwovens according to LMF content in the binder



### 4 Conclusion

ACF nonwovens were prepared using a wet-laid nonwoven process to produce a gas adsorption layer for a face mask. When ACF was immersed in water, the ammonia gas removal efficiency was reduced, even after subsequent drying. Additionally, 0.2 g ACF per 100 cm<sup>2</sup> was sufficient to obtain an ammonia gas removal efficiency of  $\geq 70\%$ . The addition of binders had no significant effect on the ammonia gas removal efficiency. With the increase in the LMF content, the tensile strength and stiffness of the ACF nonwoven increased, as did the shrinkage during the drying process. Partial melting of the LMF caused a decrease in the pore size increasing the airflow resistance, but had little effect

on the PFE. As the total binder content increased, the pore sizes of the ACF nonwovens decreased; however, the tensile strength, shrinkage during the drying process, and PFE increased. In addition, there were no meaningful changes in ammonia gas removal efficiency and particulate filtration performances after the exposure to a moist environment requested for a face mask. Filtration materials for a face mask with excellent ammonia gas removal efficiency and PFE could be obtained by the combination of ACF nonwoven with MB nonwoven. Considering the ammonia gas removal efficiency, mechanical properties, and particulate filtration performance, L5P5B40 was the most effective gas removal layer for face masks among the nonwovens assessed in this study.

**Fig. 12** Effect of humidification on the **a** PFE and **b** airflow resistance of the composite nonwovens

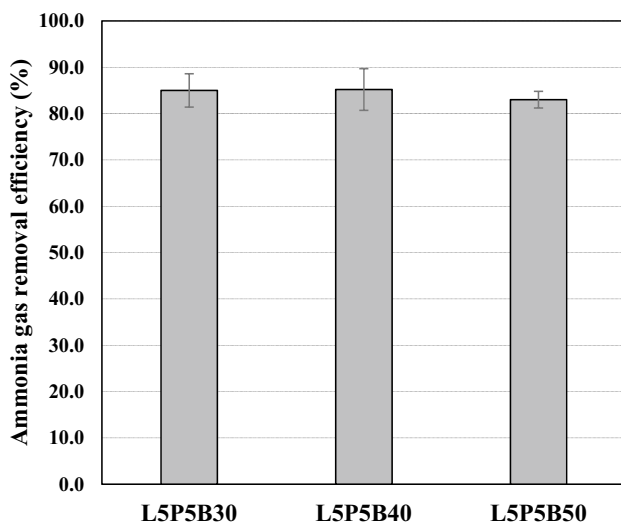
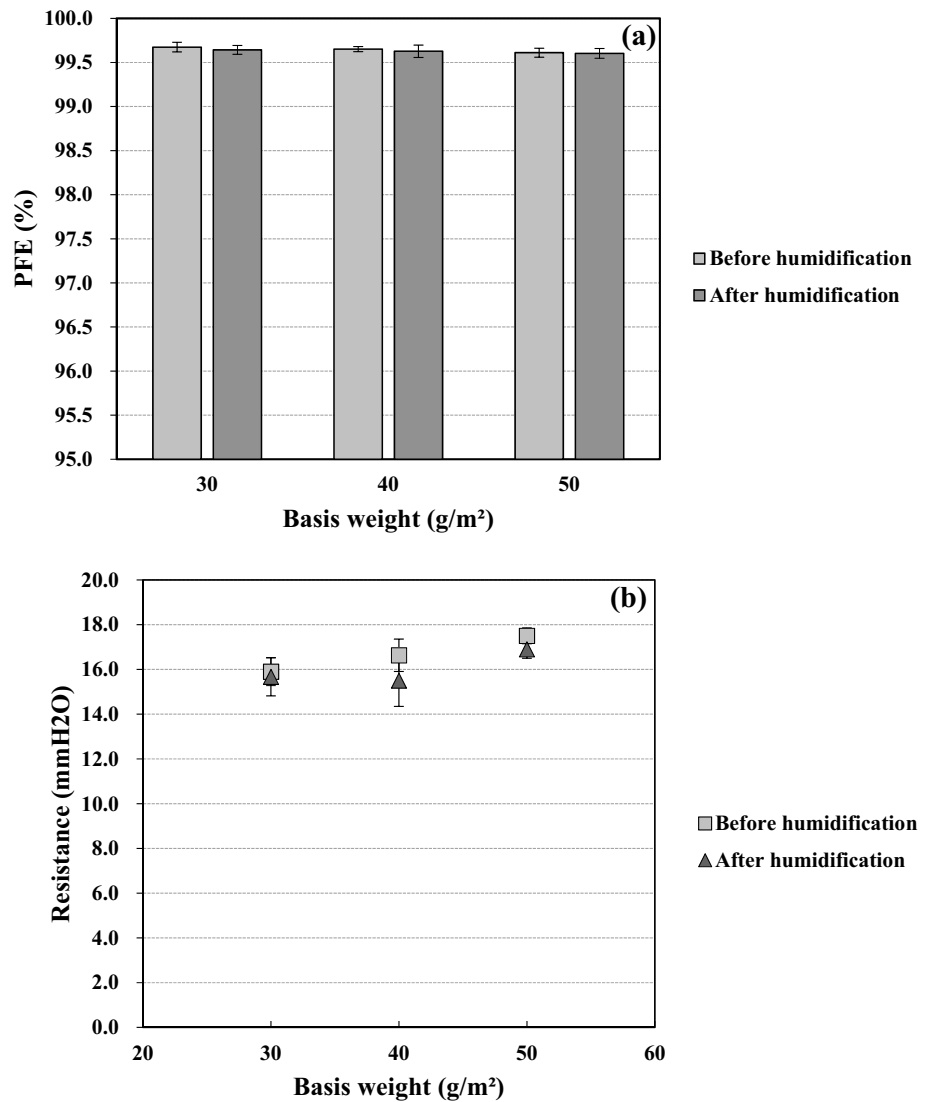


**Fig. 13** Ammonia gas removal efficiency of the composite nonwovens

**Acknowledgements** This work was supported by the Korea Institute of Industrial Technology under “Development of fiber-based technology for reduction of hazardous substances in the air” [Grant Number KITECH EO-22-0002]

**Data Availability** The data used in this research are available from the corresponding author upon reasonable request.

### Declarations

**Conflict of Interest** The authors declare that there is no conflict of interest.

### References

1. R. Barratt, R.Z. Shaban, G.L. Gilbert, *Infect. Dis. Health* **24**, 169 (2019)
2. J.E. Coia, L. Ritchie, A. Adishes, C.M. Booth, *J. Hosp. Infect.* **85**, 170 (2013)

3. C. G. Wambier, K. C. Lee, P. B. de Oliveira, S. P. de F. Wambier, and F. L. Beltrame, *J. Am. Acad. Dermatol.*, **80**, e79 (2019).
4. J.C. Clinger, P.T. O'Shaughnessy, *J. Occup. Environ. Hyg.* **16**, 423 (2019)
5. M. Harry and R. R. Francisco in "Activated carbon", 1st ed., pp.3, Elsevier, Netherlands, 2006.
6. N.M. Osmond, *Adsorpt. Sci. Technol.* **18**, 529 (2000)
7. T. Lee, C.-H. Ooi, R. Othman, F.Y. Yeoh, *Rev. Adv. Mater. Sci.* **36**, 118 (2014)
8. J.Y. Chen, N. Jiang, *J. Ind. Text.* **43**, 338 (2014)
9. T.H.C. Yeo, I.A.W. Tan, M.O. Abdullah, *Renew. Sustain. Energy Rev.* **16**, 3355 (2012)
10. D.S. Chen, W. Yan, X.Y. Zou, *Mater. Sci. Forum* **980**, 387 (2020)
11. S. Chen, Z. Hanmin, *Carbon* **41**, 1265 (2003)
12. S.J. Park, B.J. Kim, *J. Colloid Interface Sci.* **291**, 597 (2005)
13. M.A. Sidheswaran, H. Destailats, D.P. Sullivan, S. Cohn, W.J. Fisk, *Build. Environ.* **47**, 357 (2012)
14. J. Y. Chen in "Activated carbon fiber and textiles", 1st ed., pp.143–145, Woodhead Publishing, United Kingdom, 2017.
15. M.F. Hassan, M.A. Sabri, H. Fazal, A. Hafeez, N. Shezad, M. Hussain, *Anal. Appl. Pyrolysis* **145**, 104715 (2020)
16. J. Miyamoto, H. Kanoh, and K. Kaneko, *Prepr. Pap.-Am. Chem. Soc., Div. Fuel Chem.*, **50**, 1 (2005).
17. I. M. Hutten in "Handbook of nonwoven filter media", 1st ed., pp.71–102, Elsevier, Netherlands, 2007.
18. A.F. Montefusco, *Filtr. Separat.* **42**, 30 (2005)
19. W. Yim, D. Cheng, S.H. Patel, R. Kou, Y.S. Meng, J.V. Jokerst, *Acs. Appl. Mater. Inter.* **12**, 54473 (2020)
20. R. Khajavi, M.M.S. Bahadoran, A. Bahador, A. Khosravi, *J. Ind. Text* **42**, 219 (2013)
21. M. Okrasa, J. Hitz, A. Nowak, A. Brochocka, D. Thelen, Z. Walczek, *Int. J. Environ. Res. Public Health* **16**, 1973 (2019)
22. B.I. Waisi, J.T. Arena, N.E. Benes, A. Nijmeijer, R. McCutcheon, *Microporous Mesoporous Mater.* **296**, 109966 (2020)
23. K. Kawamura, K. Miyazawa, L. Kent, *AppliedChem* **1**, 14 (2021)
24. JIS K 0804:2014, Gas detector tube measurement system (Length-of-stain type), Japanese Standards Association, Tokyo, 2016.
25. TEB-APR-STP-0059, Determination of Particulate Filter Efficiency Level for N95 Series Filters Against Solid Particulates for Non-powered, Air-purifying Respirators Standard Testing Procedure, NIOSH National Personal Protective Technology Laboratory, Pittsburgh, PA, 2019.
26. S. Koji, *PCT Patent*, WO2016–167272 (2016).
27. L. Zhou, M. Li, Y. Sun, Y. Zhou, *Carbon* **37**, 773 (2001)
28. H. Abiko, F. Mitsuya, T. Takano, *Ind. Health* **48**, 427 (2010)
29. E. Hunter-Sellers, J.J. Tee, I.P. Parkin, D.R. Williams, *Microporous Mesoporous Mater.* **298**, 110090 (2020)
30. A.E. de Oliveira, M.L. Aguiar, V.G. Guerra, *Polym. Bull.* **78**, 6387 (2021)

Springer Nature or its licensor (e.g. a society or other partner) holds exclusive rights to this article under a publishing agreement with the author(s) or other rightsholder(s); author self-archiving of the accepted manuscript version of this article is solely governed by the terms of such publishing agreement and applicable law.